Asparagine Deamidation: pH-Dependent Mechanism from Density Functional Theory

Baron Peters and Bernhardt L. Trout*

Department of Chemical Engineering, Massachusetts Institute of Technology, 77 Massachusetts Avenue, Cambridge, Massachusetts 02139

Received November 29, 2005; Revised Manuscript Received March 5, 2006

ABSTRACT: Asparagine deamidation is a decisive event in chemotherapy-induced apoptosis and a major obstacle in the formulation of monoclonal antibodies. Despite the importance of deamidation, little is known about the elementary reactions involved. B3LYP/6-31+G(d,p)/COSMO-RS calculations were used to obtain stable structures and transition states for a network of reactions. Calculated rate constants were incorporated into a kinetic model of the pH dependence and compared to a pseudo-steady-state model. At low pH, the calculations show that deamidation occurs by direct acid-catalyzed hydrolysis to aspartate. At neutral to basic pH, deamidation proceeds by the initial formation of a tetrahedral intermediate. The intermediate can be converted to succinimide by two pathways and three rate-determining steps that shift in relative importance with pH. The calculated pH-dependent rate constant qualitatively agrees with the experimental pH dependence. The rate-determining transition state structures may help to understand chemotherapy-induced apoptosis and improve protein formulations.

Asparagine deamidation is a protein degradation pathway that affects biological functions (*1*−*3*), causes diseases (*2*, *4*−*9*), and degrades therapeutic proteins such as monoclonal antibodies (*10*−*17*). Despite the immense importance of asparagine deamidation, few details of the mechanism are understood. The remainder of the introduction outlines what is known about the asparagine deamidation mechanism.

Deamidation rates reach a minimum at a pH between 3 and 4 (*17*). For pH <3, deamidation is acid catalyzed with aspartate as the only product (*17*, *18*). Deamidation becomes base catalyzed for pH >4, and the products become a mixture of aspartate, isoaspartate, and cyclic succinimide residues (*17*−*21*). Scheme 1 shows the reactants and products of asparagine deamidation.

Several experiments have provided insight on the deamidation mechanism at neutral to basic conditions. Capasso and Salvadori (*22*) showed that the deamidation mechanism in a protein was the same as that in a model peptide. Capasso et al. (*19*) measured the rate of deamidation as a function of pH from 5.5 to 10 for a model pentapeptide. In addition, they found that the fully protonated states of buffers are inactive and that deprotonated buffer molecules catalyze deamidation at varying rates depending on the buffer (*19*). Capasso et al. (*20*) showed that the hydrolysis of succinimide to aspartate and isoaspartate is faster than the overall deamidation rate, so the conversion of asparagine to succinimide is the limiting step. Brennan and Clarke (*23*) showed that the rate of deamidation has a dielectric dependence that fits a generalized Born model at pH = 7.4. Because the reactant, asparagine, is neutral, the dielectric dependence indicates an ionic transition state. Patel and

Scheme 1

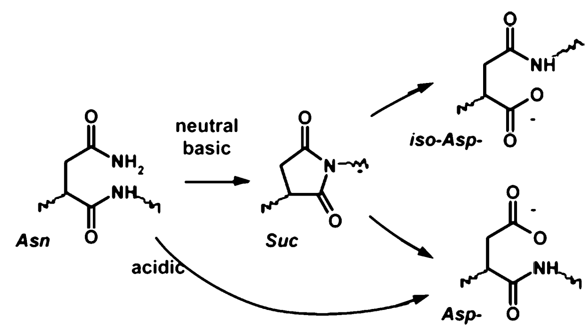

Borchardt (*24*) investigated the temperature dependence of deamidation and found an activation energy of 22 kcal/mol. Li et al. (*25*) found a small reduction in rate with solution viscosity, and Song et al. (*26*) extended the viscosity findings to proteins immobilized in glassy gels. Tyler-Cross and Schirch (*27*) and Robinson et al. (*28*) found that the residue immediately following the asparagine (on the C-terminal side) has a large effect on the deamidation rate. The fastest deamidation rates, on the time scale of a day at neutral pH, were observed for sequences containing -Asn-Gly- (*28*). Kosky et al. (*29*), Xie et al. (*30*), and Robinson et al. (*31*−*33*) found that secondary and tertiary structures generally reduce deamidation rates as compared to peptides with the same local sequence. The Robinson family developed empirical models for the effects of peptide sequence (*34*) and protein structure (*31*−*33*), and Capasso et al. (*35*) developed an empirical model for the rate of peptide deamidation that accounts for pH, temperature, buffer concentration, and sequence effects. Finally, density functional theory (DFT)[1] studies explained electronic and steric effects on the acidity of the peptide backbone (*36*), the succinimide hydrolysis mechanism (*37*), the observed isoas-

* Corresponding author. Phone: (617)-258-5021. Fax: (617)-258-5042. E-mail: trout@mit.edu.

10.1021/bi052438n CCC: $33.50
Published on Web 03/30/2006

Scheme 2

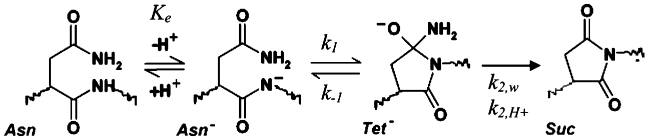

partate:aspartate ratio from succinimide hydrolysis (*38*), and the slow racemization of aspartyl and isoaspartyl products (*39*).

Despite these studies, some elementary steps of the acid- and base-catalyzed pathways remain unknown. For the base-catalyzed pathway leading to succinimide, several papers propose a deprotonation of the peptide bond nitrogen followed by a nucleophilic attack on the side chain to give a tetrahedral intermediate (*4*, *17*, *18*, *21*, *23*, *27*, *36*). On the basis of the pH dependence of succinimide formation rates, Capasso et al. proposed that there must be two pathways from the tetrahedral intermediate to succinimide (*19*). Scheme 2 shows the mechanism of succinimide formation according to Capasso et al. (*19*). Single arrows indicate steps that are assumed to be irreversible because of the scarcity of NH_3 in solution.

This computational study investigates succinimide formation and acid-catalyzed asparagine deamidation at the level of elementary steps. From a network of elementary reactions, dominant pathways and rate-limiting steps are identified at each pH. Our calculations are incorporated into a kinetic model and compared to experimental observations. Implications to chemotherapy and protein formulation are discussed.

METHODS

A network of elementary reactions was investigated using DFT. All stationary point geometries were obtained using B3LYP/6-31+G(d,p) calculations because diffuse functions are more important than extra valence functions for describing anions (*40*). Furthermore, this level of theory was adequate for previous succinimide hydrolysis studies (*37*, *38*). Saddle points were found using the growing string method (*41*) and a version of eigenvector following (*42*) with mode memory (*43*). A subset of three transition states and three minima was reoptimized at the B3LYP/6-31++G(d,p) level. The activation barriers were all within 0.5 kcal/mol of the barriers obtained from B3LYP/6-31+G(d,p) calculations, so diffuse functions on hydrogen are not necessary. All transition states have a single imaginary frequency, and all minima are vibrationally stable. The transition state structures can be seen in Appendix 1. The effect of the aqueous solvent was approximated using single point COSMO-RS (*44*) continuum solvent corrections in Gaussian03 (*45*). The dielectric changes with pH because the dielectric constant depends on the total ion concentration. Changes in the dielectric were ignored in these calculations. Free energies for all species include electronic, vibration, cavitation, and electrostatic solvation components. Rotation and translation contributions (*46*) were included for NH_3, NH_2^-, OH^-, H_2O, and H_3O^+ species. Translation and rotation of the model peptide in all states were ignored because experiments have been performed on relatively immobile pentapeptides. Contributions to the free energy of individual species and transition states are given in the Supporting Information. As in previous DFT studies (*37*−*39*, *47*), our model peptide is terminated by a methyl group and an amine as shown in Figure 1. The standard concentration of water is 55 M. All other standard concentrations are 1 M to maintain consistency with reported rate constants.

[1] Abbreviations: Asn, asparagine; Asp, aspartate; Suc, succinimide; Tet, cyclic tetrahedral intermediate; tetAsn, noncyclic tetrahedral intermediate; DFT, density functional theory; BSSE, basis set superposition error.

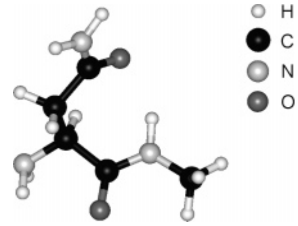

FIGURE 1: Model of an asparagine residue in a peptide. The geometry shown is the minimum energy structure. The backbone of the peptide is the $H_2N-C-C-N-CH_3$ chain along the bottom.

Experiments suggest that deamidation involves protonation and proton abstraction reactions (*17*). These reactions can often be written in multiple ways in aqueous media. In water, where $[H^+]$ and $[OH^-]$ are always related by pH + pOH = pK_w and the Gibbs free energy of water autodissociation is $-k_BT \ln[K_w]$, different ways of writing a reaction give the same equilibria. For example, AspH $\leftrightarrow$ Asp^- + H^+ and AspH + OH^- $\leftrightarrow$ Asp^- + H_2O are equivalent if the properties of water are properly treated (*48*). There are two ways to ensure results that are internally consistent. First, we could redefine K_w and the relationship between $[H^+]$ and $[OH^-]$ in water to match the computed Gibbs free energy of water autodissociation. Second, we could adjust the computed autoionization energy to match the known value for K_w. To reflect the actual properties of water, i.e., so that pH = 7 implies $[H^+] = [OH^-] = 10^{-7}$ M, we chose the latter option.

Other strategies have been developed to accurately compute pK_a values. Previous calculations of pK_as from density functional theory and continuum solvent models omit zero point correction (*49*−*52*) and scale the computed pK_as (*49*−*51*) with little justification other than an accurate value for the free energy of $H^+ + H_2O_{aq} \rightarrow H_3O^+_{aq}$ (*49*−*51*). Scale factors from COSMO-RS calculations vary from 0.60 to 0.75 depending on the model chemistry. Unfortunately, the scale factor approach presents an inconsistency for ionic transition states. Should the free energy of an ionic transition state be scaled relative to a charge neutral version of the reactants or the products?

If zero point corrections are omitted from our calculations, we obtain −255 kcal/mol for the free energy of $H^+ + H_2O_{aq} \rightarrow H_3O^+_{aq}$. This value is also within the range of experimental estimates (*51*), but we regard the agreement as fortuitous error cancellation. We note that basis set superposition errors (BSSEs) (*53*) are 12 kcal/mol for OH^- and NH_2^- using 6-311G(d,p) and only 2 kcal/mol using 6-31+G(d,p). For both basis sets, BSSEs are less important for larger anions, but BSSEs are consistently smaller for the 6-31+G(d,p) basis set. BSSE errors may partly explain the need for scale factors in pK_a calculations (*49*−*51*). Additionally, the BSSEs confirm that diffuse functions are more important than triple-ζ bases for describing anions.

Table 1: Standard Gibbs Free Energy of Reaction in kcal/mol for Reactions with Known Equilibria

	$\Delta G°$	$\Delta G°_{expt}$	error	K
$H_2O \rightleftharpoons H^+ + OH^-$	48.5	19.1	29.4	1.0E−14
$Asn \rightleftharpoons Asn^- + H^+$	51.4	21.8	29.5	1.0E−16
$Asn + OH^- \rightleftharpoons Asn^- + H_2O$	2.9	2.7	0.1	1.0E−02
$AspH \rightleftharpoons Asp^- + H^+$	26.9	5.6	21.3	7.9E−05
$AspH + OH^- \rightleftharpoons Asp^- + H_2O$	−21.6	−13.5	8.1	7.9E+09
$NH_3 \rightleftharpoons NH_2^- + H^+$	70.4	49.1	21.3	1.0E−36
$NH_3 + OH^- \rightleftharpoons NH_2^- + H_2O$	21.9	30.0	8.1	1.0E−22

Table 2: Standard Gibbs Free Energy Change in kcal/mol for Reactions with Known Equilibria with Corrections Applied to H^+ and NH_2^- Energies

	$\Delta G°$	$\Delta G°_{expt}$	error
$H_2O \rightleftharpoons H^+ + OH^-$	19.1	19.1	0.0
$Asn \rightleftharpoons Asn^- + H^+$	22.0	21.8	0.1
$Asn + OH^- \rightleftharpoons Asn^- + H_2O$	2.9	2.7	0.1
$AspH \rightleftharpoons Asp^- + H^+$	−2.5	5.6	8.1
$AspH + OH^- \rightleftharpoons Asp^- + H_2O$	−21.6	−13.5	8.1
$NH_3 \rightleftharpoons NH_2^- + H^+$	49.1	49.1	0.0
$NH_3 + OH^- \rightleftharpoons NH_2^- + H_2O$	30.0	30.0	0.0

Small ions are known to be difficult for continuum solvent models. Rather than omitting all zero point energies and scaling all computed free energy differences, we accept errors in large ions and correct the free energies of water and ammonia deprotonation as follows. Table 1 shows the calculated and experimental ΔG values for some known equilibria. Except for water autodissociation, all reactions have been written in two ways. Table 1 suggests that some ions, particularly H_3O^+ and NH_2^-, are inaccurately described by the B3LYP/6-31+G(d,p)/COSMO-RS calculations.

The free energies of water autoionization and several other reactions can be corrected by lowering the computed free energy of H_3O^+. Local and Grotthus proton transfers could delocalize the proton in solution, creating a stabilizing effect that is not captured in our DFT calculations (*54, 55*). To correct this, a −29.40 kcal/mol correction to the absolute free energy of H_3O^+ was applied to match the equilibrium constant for water autodissociation. The NH_2^- anion is particularly problematic for continuum solvent models (*50, 56*); 8.13 kcal/mol was added to the free energy of the NH_2^- in solution to match the known aqueous equilibrium of the reaction $NH_3 \leftrightarrow NH_2^- + H^+$; $pK_a = 36$ (*57*). Table 2 shows the free energies for the reactions in Table 1 after adjustment. The energies of all other species are unadjusted.

RESULTS

Figure 2 shows the reaction network that was investigated in this study. The hypothesized network includes pH-independent pathways, acid-catalyzed pathways, and base-catalyzed pathways. Succinimide hydrolysis, racemization, and interconversion of aspartate and isoaspartate are well understood from experimental and theoretical studies (*20, 21, 37−39, 58*). Furthermore, the NH_3 expulsion steps that generate the initial products are irreversible because the solution (modeled as water) does not contain NH_3. Therefore, secondary reactions involving product species were not modeled in this work.

The energy and the zero point, vibration, solvation, translation, and rotation contributions to the Gibbs free energy are given in Appendix 3. All reactions occur in liquid, so changes in volume are negligible. The Gibbs free energies of reaction and activation for reactions in the network are given in Table 3. Where water is explicitly written on both sides of the reaction, the water is actively participating in a hydrogen or proton transfer. We note that Konuklar et al. (*47*) previously investigated some portions of this network.

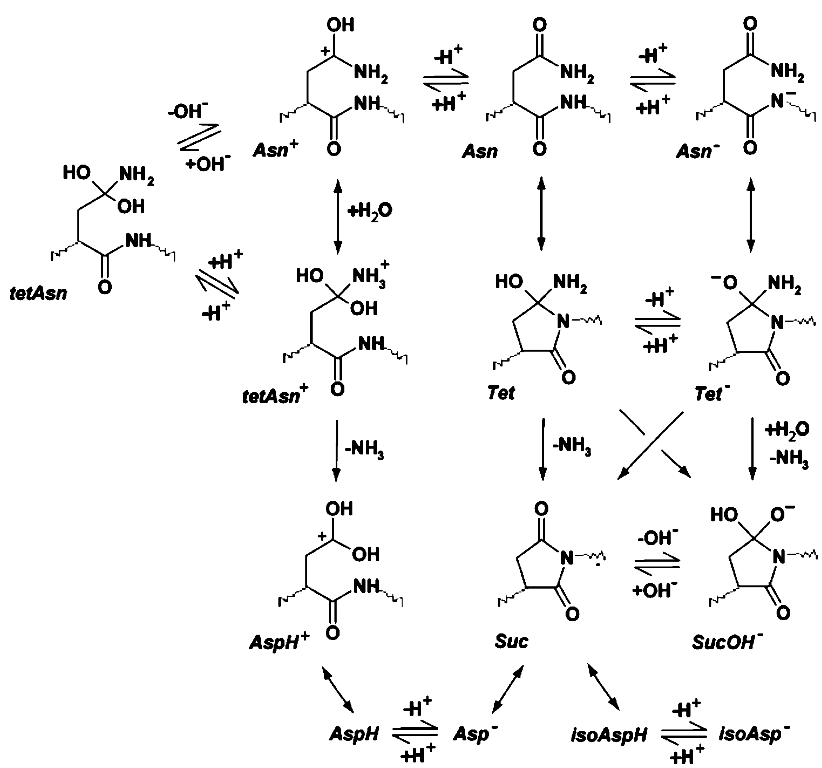

FIGURE 2: Reaction network investigated in this study. Species in equilibrium are shown with the usual symbols. Reversible but nonequilibrated reactions are shown with a double-headed arrow. Irreversible NH_3 expulsion steps are shown with a single-headed arrow.

Table 3: Standard Gibbs Free Energies of Reaction and Activation in kcal/mol

	$\Delta G°$	$\Delta G^{\ddagger}$
$H_2O \rightleftharpoons H^+ + H^-$	19.1	
$Asn + H^+ \rightleftharpoons Asn^+$	20.4	
$Asn^+ + H_2O \rightleftharpoons tetAsn^+$	4.8	30.5
$Asn^+ + OH^- \rightleftharpoons tetAsn$	−11.6	0.0
$Asn + OH^- \rightleftharpoons Asn^- + H_2O$	2.9	
$tetAsn^+ \rightleftharpoons tetAsn + H^+$	2.7	
$tetAsn^+ \rightleftharpoons AspH^+ + NH_3$	6.0	6.0
$Tet^- + H^+ \rightleftharpoons Tet + H_2O$	−14.4	
$Asn^- \rightleftharpoons Tet^-$	11.3	16.5
$Asn \rightleftharpoons Tet$	18.9	43.5
$H_2O + Asn \rightleftharpoons H_2O + Tet$	18.9	46.0
$Tet^- + H_2O \rightleftharpoons Suc + OH^- + NH_3$	−8.0	17.7
$Tet \rightleftharpoons Suc + NH_3$	−25.2	25.2
$H_2O + Tet \rightleftharpoons H_2O + Suc + NH_3$	−25.2	14.2
$AspH^+ \rightleftharpoons AspH + H^+$	−26.8	
$AspH \rightleftharpoons Asp^- + H^+$	−2.5	
$Suc + OH^- \rightleftharpoons SucOH^-$	12.4	
$Tet^- \rightleftharpoons Suc + NH_2^-$	9.6	9.6

However, Konuklar et al. did not report free energies or analyze the pH dependence resulting from their model (*47*).

The free energies of Table 3 are computed at standard conditions (pH = pOH = 1), so they do not accurately represent the conditions of aqueous solution. The actual free energy changes depend on pH according to the formula

$$\Delta G = \Delta G° + \nu_{OH^-} 2.303 k_B T(\mathrm{pH} - 14) - \nu_{H^+} 2.303 k_B T(\mathrm{pH}) \quad (1)$$

where $\Delta G°$ are the values in Table 3 and the ν_{H^+} and ν_{OH^-} are the stoichiometric coefficients of H^+ and OH^- in the reactions as written in Table 3. Equation 1 properly includes the effects of H^+ and OH^- concentration on the free energies of stable species and transition states. This treatment avoids the intuitive but incorrect assumption that base catalysis only occurs at basic pH and acid catalysis only occurs at acidic pH.

Appendix 2 includes the free energies of all stable species and transition states as functions of pH from eq 1. The table reveals the dominant pathway at each pH as the pathway from reactant to product (or succinimide) having the lowest barrier measured from the asparagine reactant. The maximum free energy along the dominant pathway is the free energy barrier. This procedure is independent of preconcieved notions that base catalysis should prevail at basic conditions. Below pH = 3, acid hydrolysis leading to aspartate is the preferred mechanism. For pH >3, mechanisms with cyclic succinimidyl intermediates become dominant. For 3 < pH < 4, the rate-limiting step is the nucleophilic attack by the deprotonated backbone of Asn^- to give the anionic tetrahedral intermediate (Tet^-). The rate-determining step is followed by reprotonation of Tet^- to give Tet. Then, water-assisted hydrogen transfer from the OH group of Tet to the NH_2 group eliminates NH_3 to give Suc. As pH increases, the free energy of the anionic transition state between Asn^- and Tet^- lowers relative to the neutral transition state between Tet and Suc. For 4 < pH < 7, the rate-limiting step becomes the water-assisted hydrogen transfer giving Suc from Tet. For pH >7, irreversible dissociation of the deprotonated Tet^- into Suc and NH_2^- becomes more favorable than the water-assisted hydrogen transfer. Figure 3 shows the network with the rate-limiting steps at each pH.

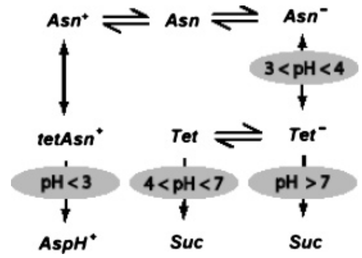

FIGURE 3: Reaction network showing how the rate-limiting step changes with pH. The Asn → Tet pathway is unimportant at all pHs, so it has been omitted.

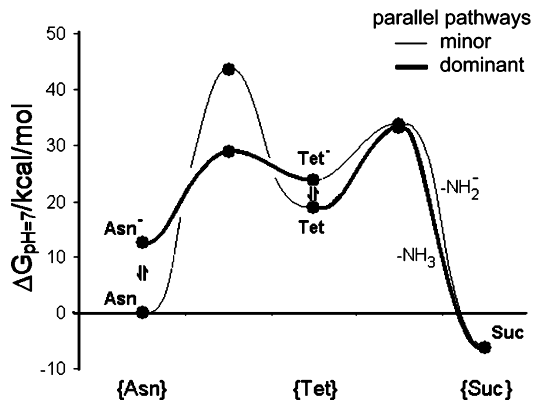

FIGURE 4: Gibbs free energy at pH = 7 measured relative to asparagines (Asn). The preferred pathway is Asn → Asn^- → Tet^- → Tet → Suc. However, dissociation of Tet^- to give Suc and NH_2^- competes with the last step. At higher pH, stabilization of the deprotonated structures makes the dissociation pathway faster than the Tet → Suc pathway.

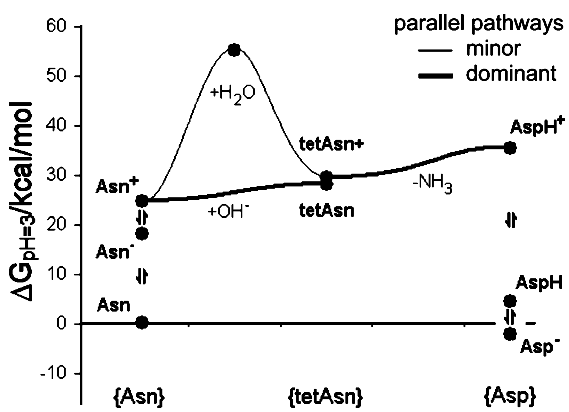

FIGURE 5: Gibbs free energy at pH = 3 measured relative to asparagine. The preferred pathway is Asn → Asn^+ → tetAsn → $tetAsn^+$ → $AspH^+$ → AspH → Asp^-, where Asp^- is aspartate.

For kinetic modeling, protonated, deprotonated, and neutral forms of each molecule can be grouped into a single basin on the potential energy surface. The NH_3 elimination steps are all irreversible, and therefore the succinimide, aspartate, and isoaspartate products can be lumped into a single product group, {P}. The grouping procedure thus results in the following groups: {Tet} = Tet and Tet^-, {tetAsn} = tetAsn and $tetAsn^+$, {Suc} = Suc and $SucOH^-$, {Asp} = Asp^-, AspH, and $AspH^+$, and {P} = {Suc}, {Asp}, and {isoAsp}, where the {isoAsp} includes the protonated and deprotonated forms of isoaspartate. Figures 4 and 5 show Gibbs free energy profiles of the two lowest free energy pathways for the base- and acid-catalyzed mechanisms, respectively. The

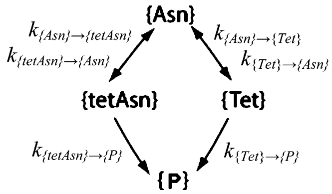

FIGURE 6: After the grouping procedure, the reaction network simplifies to two parallel pathways, the acid hydrolysis pathway (left) and the base-catalyzed succinimide pathway (right).

horizontal axes of Figures 4 and 5 are grouped reactants, intermediates, and products, but free energies of individual species within the groups are shown.

The free energy of each group can be calculated from the free energies of the individual species within the group:

$$G_{\{\mathrm{Group}\}} = -k_{\mathrm{B}}T \ln\sum_{n}\exp[-G_n/k_{\mathrm{B}}T] \tag{2}$$

Here n enumerates species within group $\{i\}$. Similarly, activation barriers from multiple pathways between groups $\{i\}$ and $\{j\}$ can be combined using

$$G^{\ddagger}_{\{i\}\to\{j\}} = -k_{\mathrm{B}}T \ln\sum_{n}\exp[-G^{\ddagger}_n/k_{\mathrm{B}}T] \tag{3}$$

where n enumerates transition states between groups $\{i\}$ and $\{j\}$. Equation 3 can be viewed as extending the dividing surface through irrelevant, high-energy portions of phase space so that it passes through each low-lying transition state. For example, Appendix 3 lists three pathways from {Asn} to {Tet}, $\mathrm{Asn}^- \to \mathrm{Tet}^-$, Asn → Tet, and a water-assisted pathway, $\mathrm{Asn} + \mathrm{H_2O} \to \mathrm{Tet} + \mathrm{H_2O}$. Therefore, $G^{\ddagger}_{\{\mathrm{Asn}\}\to\{\mathrm{Tet}\}}$ includes a Boltzmann factor for each of these three transition states. The pH-dependent activation free energies in Appendix 3 include the effects of H^+ and OH^- concentration, so apparent first-order rate constants between groups can be computed directly from eqs 4 and 5 as

$$k_{\{i\}\to\{j\}} = \frac{k_{\mathrm{B}}T}{h}\exp[-(G^{\ddagger}_{\{i\}\to\{j\}} - G_{\{i\}})/k_{\mathrm{B}}T] \tag{4}$$

The grouping procedure simplifies Figure 2 to the compact network shown in Figure 6. The reduced network has two parallel pathways, the acid hydrolysis pathway and the base-catalyzed succinimide pathway. These pathways pass through separate intermediate groups, {tetAsn} and {Tet}, respectively. The overall rate of asparagine deamidation is the sum of the rates along each of the two pathways. Using the pseudo-steady-state assumption for the intermediates gives an apparent first-order acid hydrolysis rate constant, k_{acid}, and an apparent first-order rate constant for succinimide formation, k_{base}. Figure 7 shows the results of the grouped kinetic analysis using the calculations from this work.

$$k_{\mathrm{acid}} = \frac{k_{\{\mathrm{Asn}\}\to\{\mathrm{tetAsn}\}}k_{\{\mathrm{tetAsn}\}\to\{\mathrm{P}\}}}{k_{\{\mathrm{tetAsn}\}\to\{\mathrm{P}\}} + k_{\{\mathrm{tetAsn}\}\to\{\mathrm{Asn}\}}}$$

$$k_{\mathrm{base}} = \frac{k_{\{\mathrm{Asn}\}\to\{\mathrm{Tet}\}}k_{\{\mathrm{Tet}\}\to\{\mathrm{P}\}}}{k_{\{\mathrm{Tet}\}\to\{\mathrm{P}\}} + k_{\{\mathrm{Tet}\}\to\{\mathrm{Asn}\}}} \tag{5}$$

The computed kinetics can be compared to experimental results of Capasso et al. (*19*) and Patel and Borchardt (*18*).

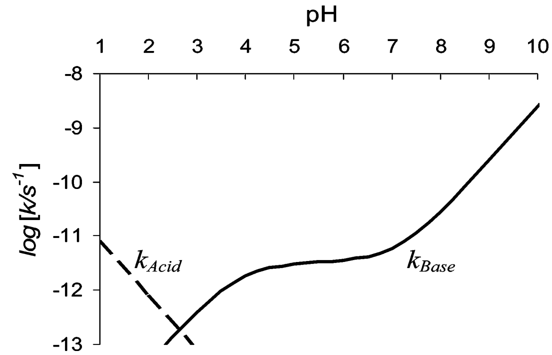

FIGURE 7: Calculated apparent first-order rate constants as functions of pH.

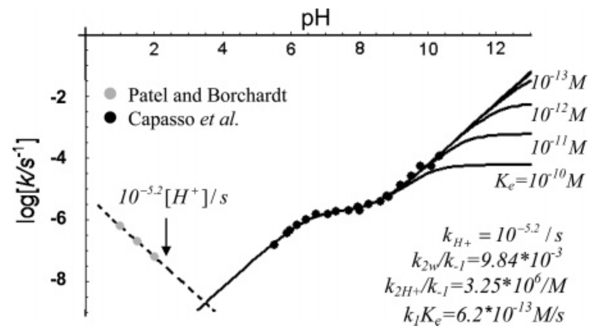

FIGURE 8: Equations 1 and 2 fitted to rate measurements from two experiments. Fitting parameters are given on the figure.

Table 4: Comparison of Fitting Parameters from Figure 8 (expt) to the Analogous Calculated Parameters (calc)[a]

	expt	calc
$k_{2\mathrm{W}}/k_{-1}$	9.8×10^{-3}	5.7×10^{-4}
$k_{2\mathrm{H}^+}/k_{-1}$	3.3×10^{6}	7.5×10^{3}
k_1K_e	6.2×10^{-13}	4.4×10^{-16}
k_{H^+}	6.3×10^{-6}	7.9×10^{-11}

[a] Units are as shown in Figure 8.

The psuedo-steady-state hypothesis applied to the asparagine deamidation mechanism of Scheme 2 gives an apparent deamidation rate constant of the form

$$k_{\mathrm{Asn}\to\mathrm{Suc}} = \frac{k_1K_\mathrm{e}}{K_\mathrm{e} + [\mathrm{H}^+]}\left(1 - \frac{1}{1 + (k_{2,\mathrm{w}} + k_{2,\mathrm{H}}[\mathrm{H}^+])/k_{-1}}\right) \tag{6}$$

A similar expression in Capasso et al. (*20*) for the equilibration of aspartate and isoaspartate via succinimide contains a typographical error. The low pH data of Patel and Borchardt (*18*) suggest a pH-dependent rate constant of the form

$$k_{\mathrm{acid}} = k_{\mathrm{H}^+}[\mathrm{H}^+] \tag{7}$$

Figure 8 shows the deamidation rate data of Capasso et al. (*19*) and Patel and Borchardt (*18*) with curves from fitting (6) and (7) to the measured deamidation rates. Figure 8 also shows the fitting parameters that generated the curves. Comparison of Figures 7 and 8 shows that the computed pH dependence qualitatively resembles the experimental pH dependence. However, the computed rate constants are nearly 5 orders of magnitude too small. Table 4 compares the experimental fitting parameters to the analogous calculated parameters.

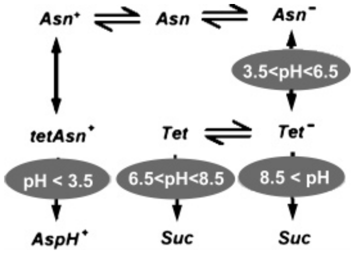

FIGURE 9: Rate-determining steps as functions of pH can be inferred from the correspondence between calculated and observed kinetics.

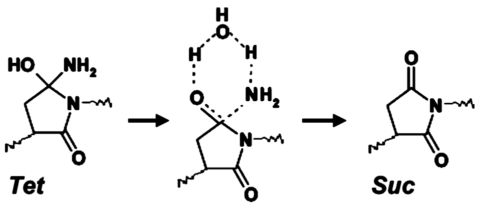

FIGURE 10: Rate-determining step and transition state at pH = 7.4. A more detailed transition state structure is shown in Appendix 1.

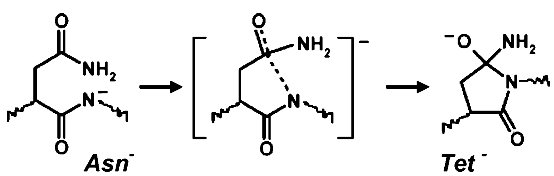

FIGURE 11: Rate-determining step and transition state for 4 < pH < 6. A more detailed transition state structure is shown in Appendix 1.

The errors in the rates correspond to a 7 kcal/mol error in the activation energy. The error likely originated from the COSMO-RS solvent model. COSMO-RS, like many continuum solvent models, creates the solvent cavity from overlapping spheres centered at the nuclei (*44*, *56*). Electron density contours of transition state wave functions may deviate significantly from the piecewise spherical boundary. COSMO-RS partially accounts for tails of the wave function that extend beyond the cavity with a second cavity boundary (*44*), but severely distorted transition state orbitals may still lead to erroneous solvent corrections.

We note that calculated pK_as from the self-consistent isodensity polarizable continuous medium (SCI-PCM) solvent model (*59*) scale very closely with experimental pK_as (*51*, *52*). Because the SCI-PCM cavity is the isodensity surface of the polarized solute, SCI-PCM should work equally well for transition states. Unfortunately, SCI-PCM was last implemented in Gaussian94 and, to our knowledge, is unavailable in other electronic structure packages (*59*).

The calculated rate-determining steps can be reassigned to experimental pH ranges using the correspondence between the calculated and observed pH dependence. Figure 9 shows the reduced network of Figure 3 with inferred pH ranges. Figures 10 and 11 show the inferred transition states for the rate-determining steps at pH = 7.4 and 4 < pH < 6. These pH values approximately correspond to in vivo deamidation conditions (*4*) and protein formulation conditions (*60*).

At pH = 7.4 the transition state along the rate-determining step involves a water-assisted hydrogen transfer. The water-assisted transition state may explain how the antiapoptic protein Rb suppresses Bcl-x_L deamidation in cells subjected to chemotherapy (*8*, *9*). Recent findings suggest there are more pathways that conditionally allow Bcl-x_L deamidation to control apoptosis (*3*). At biological pH, steric interference with the water-assisted hydrogen transfer is sufficient to suppress deamidation. The water-assisted mechanism may also explain the suppressed deamidation of asparagine residues with bulky C-terminal neighbors. Steric effects should be less pronounced for 4 < pH < 5 than for pH = 7.4 where most sequence effects have been measured (*24*, *27*, *28*, *61*). For the anionic intramolecular transition state that is limiting at mildly acidic pH, electronic properties of the neighboring C-terminal residue and the solution will be important. In particular, the deamidation rate should decrease with decreasing solvent dielectric.

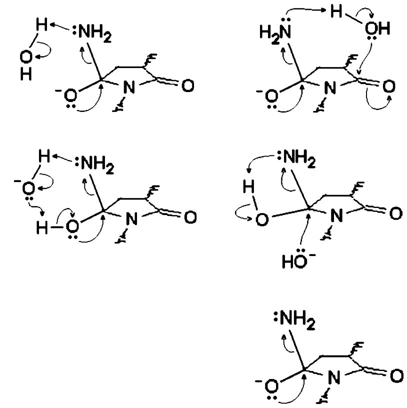

FIGURE 12: Five pathways were explored linking Tet and Tet− to succinimide species. Surprisingly, the calculations suggest that the preferred pathway is an irreversible NH_2^- dissociation. In water, this would be followed by a kinetically invisible reduction to NH_3.

For pH >8.5, NH_2^- dissociation from Tet− was not the expected transition state. We anticipated that a water molecule would donate a proton to facilitate the leaving of the NH_2 group from Tet− or that an incoming OH^- and a concerted proton transter from the OH group of Tet would displace an NH_3 molecule from Tet. Several of the transition states that we explored are shown in Figure 12. The upper two transition states in Figure 12 show H_2O donating a proton to help to eliminate NH_3 from Tet−. These transition states were of higher energy than direct elimination of NH_2^- from Tet−. The middle row of transition states in Figure 12 show OH^- attacking neutral Tet while Tet simultaneously eliminates NH_3. These transition states could only be obtained using simplified models of the peptide with the C-terminal backbone terminated by hydrogen instead of a methyl group. (See Figure 1.) Transition state searches with the full peptide model resulted in a succinimidyl peptide with a nearby proton transfer occurring between water and NH_2^-. The inability to find an OH^- attack on neutral Tet may indicate that the gas-phase transition states are significantly different from the liquid-phase transition states and that a more sophisticated treatment of the aqueous environment is needed. However, it could indicate that the reaction does proceed through an initial dissociation of NH_2^- followed by a rapid NH_2^- reduction. The five mechanisms cannot be distinguished by labeling studies. However, the dissociation mechanism should have the smallest kinetic isotope effect in deuterated water because the other four elementary reactions are hydrogen transfers.

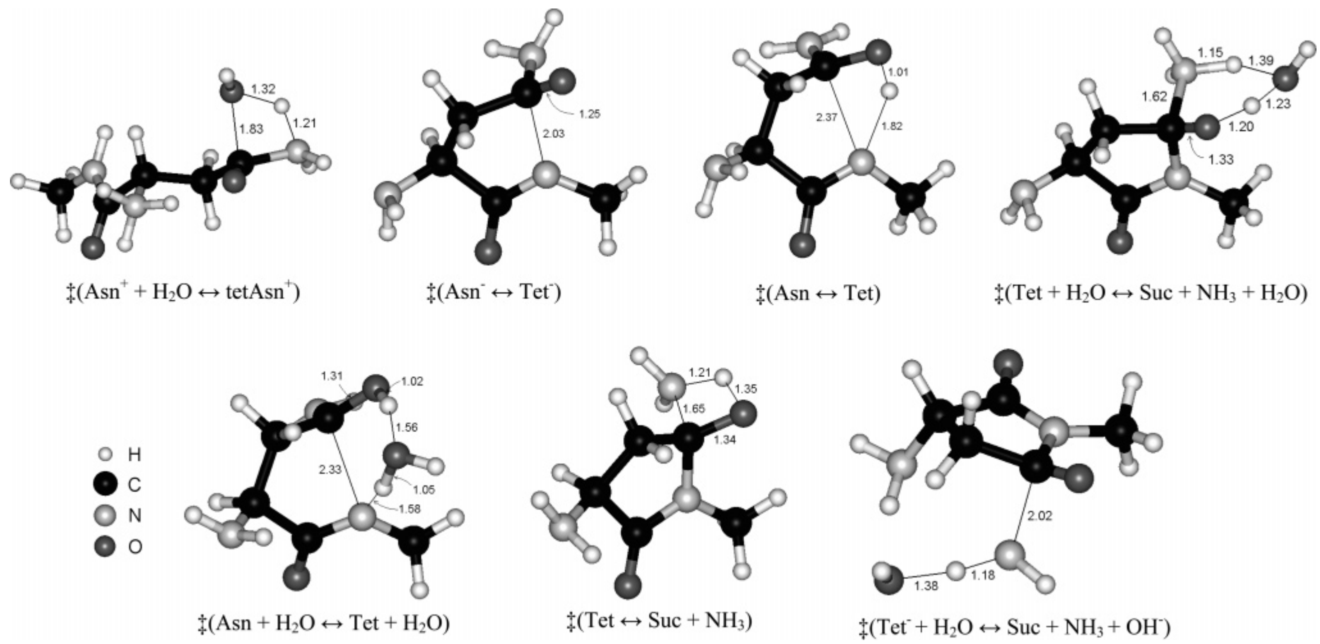

FIGURE 13: B3LYP/6-31+G(d,p) transition state structures with atoms colored according to the key at the left. The transition states are labeled according to their reactants and products. Distances are given in angstroms.

Table 5: Gibbs Free Energies of Stable Species and Transition States in kcal/mol Relative to the Free Energy of Asparagine[a]

pH:	1	2	3	4	5	6	7	8	9	10	11	12	13
Asn^-	20.6	19.2	17.9	16.5	15.1	13.8	12.4	11.0	9.7	8.3	6.9	5.6	4.2
Asn	**0.0**	**0.0**	**0.0**	**0.0**	**0.0**	**0.0**	**0.0**	**0.0**	**0.0**	**0.0**	**0.0**	**0.0**	**0.0**
Asn^+	21.7	23.1	24.5	25.8	27.2	28.6	29.9	31.3	32.7	34.0	35.4	36.7	38.1
‡(Asn- ↔ Tet^-)	37.0	35.7	**34.3**	32.9	31.6	30.2	28.9	27.5	26.1	24.8	23.4	22.0	20.7
‡(Asn ↔ Tet)	43.5	43.5	43.5	43.5	43.5	43.5	43.5	43.5	43.5	43.5	43.5	43.5	43.5
‡(Asn+H_2O↔Tet+H_2O)	46.0	46.0	46.0	46.0	46.0	46.0	46.0	46.0	46.0	46.0	46.0	46.0	46.0
Tet^-	31.9	30.6	29.2	27.8	26.5	25.1	23.7	22.4	21.0	19.6	**18.3**	**16.9**	**15.5**
Tet	**18.9**	**18.9**	**18.9**	**18.9**	**18.9**	**18.9**	**18.9**	**18.9**	**18.9**	**18.9**	18.9	18.9	18.9
‡(Tet^- + H_2O ↔ Suc+OH^-+NH_3)	49.6	48.3	46.9	45.5	44.2	42.8	41.4	40.1	38.7	37.3	36.0	34.6	33.2
‡(Tet^- ↔ Suc+NH_2^-)	41.5	40.1	38.7	37.4	36.0	34.6	33.3	**31.9**	**30.6**	**29.2**	**27.8**	**26.5**	**25.1**
‡(Tet ↔ Suc+NH_3)	44.1	44.1	44.1	44.1	44.1	44.1	44.1	44.1	44.1	44.1	44.1	44.1	44.1
‡(H_2O+Tet ↔ Suc+H_2O+NH_3)	33.1	33.1	33.1	**33.1**	**33.1**	**33.1**	**33.1**	33.1	33.1	33.1	33.1	33.1	33.1
$SucOH^-$	23.9	22.5	21.2	19.8	18.4	17.1	15.7	14.4	13.0	11.6	10.3	8.9	7.5
Suc	**-6.3**	**-6.3**	**-6.3**	**-6.3**	**-6.3**	**-6.3**	**-6.3**	**-6.3**	**-6.3**	**-6.3**	**-6.3**	**-6.3**	**-6.3**
‡(Asn^++OH- ↔ tetAsn)	27.9	27.9	27.9	27.9	27.9	28.6	29.9	31.3	32.7	34.0	35.4	36.7	38.1
‡(Asn^+ +H_2O ↔ $tetAsn^+$)	52.2	53.6	54.9	56.3	57.7	59.0	60.4	61.7	63.1	64.5	65.8	67.2	68.6
$tetAsn^+$	**26.6**	**27.9**	29.3	30.7	32.0	33.4	34.8	36.1	37.5	38.8	40.2	41.6	42.9
tetAsn	27.9	27.9	**27.9**	**27.9**	**27.9**	**27.9**	**27.9**	**27.9**	**27.9**	**27.9**	**27.9**	**27.9**	**27.9**
‡($tetAsn^+$ ↔ $AspH^+$ + NH_3)	**32.6**	**34.0**	35.3	36.7	38.1	39.4	40.8	42.2	43.5	44.9	46.2	47.6	49.0
$AspH^+$	32.6	34.0	35.3	36.7	38.1	39.4	40.8	42.2	43.5	44.9	46.2	47.6	49.0
AspH	4.4	4.4	4.4	4.4	4.4	4.4	4.4	4.4	4.4	4.4	4.4	4.4	4.4
Asp^-	**0.5**	**-0.8**	**-2.2**	**-3.6**	**-4.9**	**-6.3**	**-7.7**	**-9.0**	**-10.4**	**-11.7**	**-13.1**	**-14.5**	**-15.8**

[a] Within each equilibrated group, e.g., {Asn} = Asn^+, Asn, and Asn^-, the free energy of the dominant species is outlined in gray. Similarly, the rate-limiting transition state at each pH is indicated by a black background. Species on the base- and acid-catalyzed pathways are separated from each other and from {Asn} by double lines.

DISCUSSION

We present, for the first time, detailed mechanisms of elementary steps for the deamidation of asparagine residues by acid and base catalysis. The elementary steps in our mechanism yield overall rates that qualitatively agree with the experimental rates as a function of pH. Our calculations show that the minimum rate of deamidation occurs at approximately pH = 3. For pH <3, acid catalysis yields aspartate through a sequence of reactions that result in an $-NH_3^+$ leaving group. For pH >3, base catalysis leads to succinimide which then hydrolyzes to aspartate and isoaspartate products. Base catalysis begins with the deprotonation of the peptide nitrogen on the neighboring C-terminal residue. After the initial step, the calculations predict three mechanisms for succinimide formation depending on the pH. For mildly acidic conditions, the rate-limiting step is an intramolecular nucleophilic attack on the side chain carbonyl by the deprotonated nitrogen. For neutral pH, a water-assisted hydrogen transfer reaction is the rate-limiting step. For basic conditions, direct elimination of NH_2^- from the anionic tetrahedral intermediate is rate limiting.

The rate-limiting water-assisted hydrogen transfer step at neutral pH has implications for chemotherapy-induced apoptosis. The antiapoptic protein Rb could prevent Bcl-x_L deamidation by binding to Bcl-x_L in a way that interferes with the water-assisted transfer. Similarly, some sequence effects at neutral pH could be explained as steric interference with the water-assisted transition state. Steric effects may be less important for protein formulations which are prepared at mildly acidic pH where the rate-limiting step is intramolecular. Because the intramolecular transition state is anionic, a low solvent dielectric constant may stabilize protein formulations.

ACKNOWLEDGMENT

The authors thank Bernard R. Brooks, H. Lee Woodcock, and the reviewers for suggestions on basis sets and solvent models. Additionally, we thank Louis Clark and Bin Pan for discussions about deamidation.

APPENDIX 1

Saddle point structures are shown in Figure 13.

APPENDIX 2

Gibbs free energies as functions of pH are shown in Table 5.

SUPPORTING INFORMATION AVAILABLE

One table giving the individual components of the total Gibbs free energy. This material is available free of charge via the Internet at http://pubs.acs.org.

REFERENCES

1. Weintraub, S. J., and Manson, S. R. (2004) Asparagine deamidation: a regulatory hourglass, *Mech. Ageing Dev. 125*, 255−257.
2. Robinson, N. E., and Robinson, A. B. (2001) Deamidation as a molecular clock, *Proc. Natl. Acad. Sci. U.S.A. 98*, 944.
3. Zhao, R., Yang, F. T., and Alexander, D. R. (2004) An oncogenic tyrosine kinase inhibits DNA repair and DNA-damage-induced Bcl-xL deamidation in T cell transformation, *Cancer Cell 5*, 37−49.
4. Reissner, K. J., and Aswad, D. W. (2003) Deamidation and isoaspartate formation in proteins: unwanted alterations or surreptitious signals?, *Cell. Mol. Life Sci. 60*, 1281−1295.
5. Goldberg, R. J. (2003) Protein degradation and protection against misfolded or damaged proteins, *Nature 426*, 895−899.
6. Hoenders, H. J., and Bloemendal, H. (1983) Lens proteins and aging, *J. Gerontol. 38*, 278−286.
7. Nilsson, M. R., Driscoll, M., and Raleigh, D. P. (2002) Low levels of asparagine deamidation can have a dramatic effect on aggregation of amyloidogenic peptides: Implications for the study of amyloid formation, *Protein Sci. 11*, 342−349.
8. Li, C., and Thompson, C. B. (2002) DNA damage, deamidation, and death, *Science 298*, 1346−1347.
9. Deverman, B. E., Cook, B. L., Manson, S. R., Niederhoff, R. A., Langer, E. M., Rosova, I., Kulans, X. Y., Fu, J. S., Weinberg, J. S., Heinecke, J. W., Roth, K. A., and Weintraub, S. J. (2002) Bcl-xL deamidation is a critical switch in the regulation of the response to DNA damage, *Cell 111*, 51−62.
10. Goldenberg, D. M. (2001) The role of radiolabeled antibodies in the treatment of non-Hodgkin's lymphoma: the coming of age of radioimmunotherapy, *Crit. Rev. Oncol. Hematol. 39*, 195−201.
11. Senter, P. D., and Springer, C. J. (2001) Selective activation of anticancer prodrugs by monoclonal antibody-enzyme conjugates, *Adv. Drug Delivery Rev. 53*, 247−264.
12. Burtrum, D., Zhu, Z., Lu, D., Anderson, D. M., Prewett, M., Pereira, D. S., Bassi, R., Abdullah, R., Hooper, A. T., Koo, H., Jimenez, X., Johnson, D., Apblett, R., Kussie, P., Bohlen, P., Witte, L., Hicklin, D. J., and Ludwig, D. L. (2003) A fully human monoclonal antibody to the insulin-like growth factor I receptor blocks ligand dependent signaling and inhibits tumor growth in vivo, *Cancer Res. 63*, 8912−8921.
13. Trikha, M., Corringham, R., Klein, B., and Rossi, J.-F. (2003) Targeted anti-interleukin-6 monoclonal antibody therapy for cancer, *Clin. Cancer Res. 9*, 4653−4665.
14. Dadachova, E., Nosanchuk, J. D., Shi, L., Schweitzer, A. D., Frenkel, A., Nosanchuk, J. S., and Casadevall, A. (2004) Dead cells in melanoma tumors provide abundant antigen for targeted delivery of ionizing radiation by a mAb to melanin, *Proc. Natl. Acad. Sci. U.S.A. 101*, 14865−14870.
15. Ko, K., Steplewski, Z., Glogowska, M., and Koprowski, H. (2005) Inhibition of tumor growth by plant-derived mAb, *Proc. Natl. Acad. Sci. U.S.A. 102*, 7026−7030.
16. Huang, L., Lu, J., Wroblewski, V. J., Beals, J. M., and Riggin, R. M. (2005) In vivo deamidation characterization of monoclonal antibody by LC/MS/MS, *Anal. Chem. 77*, 1432−1439.
17. Brennan, T. V., and Clarke, S. (1995) Deamidation and isoaspartate formation in model synthetic peptides: The effects of sequence and solution environment, in *Deamidation and Isoaspartate Formation in Peptides and Proteins* (Aswad, D. W., Ed.) pp 65−90, CRC Press, Boca Raton, FL.
18. Patel, K., and Borchardt, R. T. (1990) Chemical pathways of peptide degradation. II. Kinetics of deamidation of an asparaginyl residue in a model hexapeptide, *Pharm. Res. 7*, 703−711.
19. Capasso, S., Mazzarella, L., Sica, F., Zagari, A., and Salvadori, S. (1993) Kinetics and mechanism of succinimide ring formation in the deamidation process of asparagine residues, *J. Chem. Soc., Perkin Trans. 2*, 679−682.
20. Capasso, S., Kirby, A. J., Salvadori, S., Sica, F., and Zagari, A. (1995) Kinetics and mechanism of the reversible isomerization of aspartic acid residues in tetrapeptides, *J. Chem. Soc., Perkin Trans. 2*, 437−442.
21. Lura, R., and Schirch, V. (1988) Role of peptide conformation in the rate and mechanism of deamidation of asparaginyl residues, *Biochemistry 27*, 7671−7677.
22. Capasso, S., and Salvadori, S. (1999) Effect of the three-dimensional structure on the deamidation reaction of ribonuclease A, *J. Pept. Res. 54*, 377−382.
23. Brennan, T. V., and Clarke, S. (1993) Spontaneous degradation of polypeptides at aspartyl and asparaginyl residues: Effects of the solvent dielectric, *Protein Sci. 2*, 331−338.
24. Patel, K., and Borchardt, R. T. (1990) Chemical pathways of peptide degradation. III. Effect of primary sequence on the pathways of deamidation of asparaginyl residues in hexapeptides, *Pharm. Res. 7*, 787−793.
25. Li, R., D'Souza, A. J., Laird, B. B., Schowen, R. L., Borchardt, R. T., and Topp, E. M. (2000) Effects of solution polarity and viscosity on peptide deamidation, *J. Pept. Res. 56*, 326−333.
26. Song, Y., Schowen, R. L., Borchardt, R. T., and Topp, E. M. (2001) Effect of "pH" on the rate of asparagine deamidation in polymeric formulations: "pH"-rate profile, *J. Pharm. Sci. 90*, 141−156.
27. Tyler-Cross, R., and Schirch, V. (1991) Effects of amino acid sequence, buffers, and ionic strength on the rate and mechanism of deamidation of asparagine residues in small peptides, *J. Biol. Chem. 266*, 22549−22556.
28. Robinson, N. E., Robinson, Z. W., Robinson, B. R., Robinson, A. L., Robinson, J. A., Robinson, M. L., and Robinson, A. B. (2004) Structure-dependent nonenzymatic deamidation of glutaminyl and asparaginyl pentapeptides, *J. Pept. Res. 63*, 426−436.
29. Kosky, A. A., Razzaq, U. O., Treuheit, M. J., and Brems, D. N. (1999) The effects of alpha-helix on the stability of Asn residues: Deamidation rates in peptides of varying helicity, *Protein Sci. 8*, 2519−2523.
30. Xie, M., Shahrokh, Z., Kadkhodayan, M., Henzel, W. J., Powell, M. F., Borchardt, R. T., and Schowen, R. L. (2002) Asparagine deamidation in recombinant human lymphotoxin: Hindrance by three-dimensional structures, *J. Pharm. Sci. 92*, 869−880.
31. Robinson, N. E., and Robinson, A. B. (2001) Predicting deamidation rates of human proteins from 3D structures, *Proc. Natl. Acad. Sci. U.S.A. 98*, 12409.
32. Robinson, N. E. (2002) Protein deamidation, *Proc. Natl. Acad. Sci. U.S.A. 99*, 5283−5288.
33. Robinson, N. E., and Robinson, A. B. (2001) Prediction of protein deamidation rates from primary and three-dimensional structure, *Proc. Natl. Acad. Sci. U.S.A. 98*, 4367−4372.

34. Robinson, N. E., and Robinson, A. B. (2004) Prediction of primary structure deamidation rates of asparaginyl and glutaminyl peptides through steric and catalytic effects, *J. Peptide Res. 63*, 437−448.
35. Capasso, S. (2000) Estimation of the deamidation rate of asparagine side chains, *J. Pept. Res. 55*, 224−229.
36. Radkiewicz, J. L., Zipse, H., Clarke, S., and Houk, K. N. (2001) Neighboring side chain effects on asparaginyl and aspartyl degradation: An ab initio study of the relationship between peptide conformation and backbone NH acidity, *J. Am. Chem. Soc. 123*, 3499−3506.
37. Konuklar, F. A., Aviyente, V., and Ruiz-Lopez, M. F. (2002) Theoretical study on the alkaline and neutral hydrolysis of succinimide derivatives in deamidation reactions, *J. Phys. Chem. A 106*, 11205−11214.
38. Konuklar, F. A., and Aviyente, V. (2003) Modelling the hydrolysis of succinimide: formation of aspartate and reversible isomerization of aspartic acid via succinimide, *Org. Biomol. Chem. 1*, 2290−2297.
39. Radkiewicz, J. L., Zipse, H., Clarke, S., and Houk, K. N. (1996) Accelerated racemization of aspartic acid and asparagine residues via succinimide intermediates: An ab Initio theoretical exploration of mechanism, *J. Am. Chem. Soc. 118*, 9148−9155.
40. Lynch, B. J., Zhao, R., and Truhlar, D. G. (2003) Effectiveness of diffuse basis functions for calculating relative energies by density functional theory, *J. Phys. Chem. A 107*, 1384−1388.
41. Peters, B., Heyden, A., Bell, A. T., and Chakraborty, A. K. (2004) A growing string method for the location of transition states: Comparison to the nudged elastic band and string methods, *J. Chem. Phys. 120*, 7877−7886.
42. Baker, J. (1986) An algorithm for the location of transition states, *J. Comput. Chem. 7*, 385−395.
43. Shao, Y. (2006) Q-Chem 3.0: A high performance quantum chemistry package for molecular electronic structure calculations, *Phys. Chem. Chem. Phys.* (in press).
44. Klamt, A., Jonas, V., Burger, T., and Lohrenz, J. C. W. (1998) Refinement and parameterization of COSMO-RS. *J. Phys. Chem. A 102*, 5074−5085.
45. Frisch, M. J. (2003) Gaussian Inc., Wallingford, CT.
46. Laidler, K. J., and Meiser, J. H. (1982) *Physical Chemistry*, Benjamin Cummings, Menlo Park, CA.
47. Konuklar, F. A., Aviyente, V., Sen, T. Z., and Bahar, I. (2001) Modeling the deamidation of asparagine residues via succinimide intermediates, *J. Mol. Model. 7*, 147−160.
48. Tinoco, I., Sauer, K., Wang, J. C., and Puglisi, J. D. (2001) *Physical Chemistry: Principles and Applications in Biological Sciences*, 4th ed., Prentice Hall, Upper Saddle River, NJ.
49. Klamt, A., Eckert, F., Diedenhofer, M., and Beck, M. E. (2003) First principles calculations of aqueous pK_a values for organic and inorganic acids using COSMO-RS reveal an inconsistency in the slope of the pK_a scale, *J. Phys. Chem. A 107*, 9380−9386.
50. Klamt, A., and Eckert, F. (2005) Accurate prediction of basicity in aqueous solution with COSMO-RS, *J. Comput. Chem. 27*, 11−19.
51. Kallies, B., and Mitzner, R. (1997) pK_a values of amines in water from quantum mechanical calculations using a polarized dielectric continuum representation of the solvent, *J. Phys. Chem. A 101*, 2959−2967.
52. Himo, F., Noodleman, L., Blomberg, M. R. A., Siegbahn, P. E. M.,. (2002) Relative acidities of ortho-substituted phenols as models for modified tyrosines in proteins, *J. Phys. Chem. A 106*, 8757−8761.
53. Boys, S. F., and Bernardi, F. (1970) The calculation of small molecular interactions by differences of separate total energies. Some procedures with reduced errors, *Mol. Phys. 19*, 553−566.
54. Trout, B. L., and Parinello, M. (1998) The dissociation mechanism of H_2O in water studied by first-principles molecular dynamics, *Chem. Phys. Lett. 288*, 343−346.
55. Sprik, M. (2000) Ab initio molecular dynamics simulation of liquids and solutions, *J. Phys. Condens. Matter 12*, A161−A163.
56. Cramer, C., and Truhlar, D. G. (1999) Implicit solvation models: equilibria, structure, and dynamics, *Chem. Rev. 99*, 2161−2200.
57. Bruice, P. Y. (2002) *Organic Chemistry*, 4th ed., Prentice Hall, Upper Saddle River, NJ.
58. Xie, M., Vander Velde, D., Morton, M., Borchardt, R. T., and Schowen, R. L. (1996) pH-induced change in the rate-determining step for the hydrolysis of the Asp/Asn-derived cyclic-imide intermediate in protein degradation, *J. Am. Chem. Soc. 118*, 8955−8956.
59. Foresman, J. B., Keith, T. A., Wiberg, K. B., Snoonian, J., and Frisch, M. J. (1996) Solvent effects. 5. Influence of cavity shape, truncation of electrostatics, and electron correlation on ab initio reaction field calculations, *J. Phys. Chem. 100*, 16098−16104.
60. Speed-Ricci, M. (2005) personal communication.
61. Geiger, T., and Clarke, S. (1987) Succinimide linked reactions that contribute to protein degradation, *J. Biol. Chem. 262*, 785−794.

BI052438N